WARSAW UNIVERSITY OF TECHNOLOGY Index 351733
FACULTY OF CIVIL ENGINEERING
COMMITTEE FOR CIVIL AND WATER ENGINEERING
POLISH ACADEMY OF SCIENCES ISSN 1230-2945
DOI: 10.24425/ace.2024.151905
ARCHIVES OF CIVIL ENGINEERING
Vol. LXX ISSUE 4 2024
pp. 491 –503

Research paper

Safety management of deep excavation engineering in subway stations based on soil mechanics response simulation analysis

Deqiu Zhang[1], Jingyan Wang[2]

Abstract: As the economy develops with the continuous acceleration of modern urban construction, the demand for subway construction has been increasing. When constructing subway stations, the safety management of deep foundation pit support engineering is particularly important. To balance the absolute safety and economic benefits of subway station construction projects, the safety management of subway station deep excavation projects based on soil mechanics response simulation analysis is studied. Taking the deep foundation pit project of Wuhan Metro Station as an example, this study uses numerical simulation analysis technology and actual monitoring data to conduct in-depth analysis of the deformation of the deep foundation pit. Meanwhile, through finite element technology, the influence of internal support system structural parameters on deep foundation pit deformation in deep foundation pit support engineering is studied, and the parameters of the original support structure are optimized. Results showed that the maximum horizontal displacement of the original scheme reached 25.7 mm, while that of the optimized parameter scheme was only 18.6 mm, which is a decrease of 27.62% compared to the original scheme. In summary, the research on safety management of subway station deep foundation pit engineering based on soil mechanics response simulation analysis is important in promoting the development of modern urban subway construction.

Keywords: soil mechanics, deep foundation pit engineering, safety management, finite element technology, subway station

[1]MsC., School of Civil Engineering, Harbin University, Harbin, 150000, China, e-mail: zhangdeqiu2022@126.com, ORCID: 0009-0006-3326-6173

[2]PhD., School of Civil Engineering, Harbin University, Harbin, 150000, China, e-mail: wangjingyan202208@126.com, ORCID: 0009-0002-3381-904X

1. Introduction

The continuous growth of urban population has gradually increased traffic pressure, and subway transportation, as an effective way to solve this problem, is increasingly highlighting its importance in urban development and construction [1]. Due to the fact that subway stations are usually located at hubs connecting various bustling areas of the city, the surrounding environment of their construction sites is often very complex [2]. Therefore, subway construction projects need to consider many factors, such as hydrogeology, road traffic, surrounding environmental protection, and economic benefits. However, the underground excavation work of subway engineering projects inevitably leads to deformation or displacement of the surrounding soil, which may have an impact on the surrounding buildings [3]. If the deep foundation pit (DFP) design is improper, it may lead to construction accidents. Therefore, the design of subway station deep foundation pit (SSDFP) support is extremely important in constructing subway stations. Meanwhile, overly conservative design of SSDFP support may lead to resource waste and increased construction costs [4, 5].This article analyzes the results of excavation of foundation pits using numerical simulation techniques and optimizes the original design based on this. The research value obtained can provide reference basis for the selection of support design parameters for similar subway foundation pit projects in the future. Therefore, this study has extremely important engineering experience accumulation and engineering application value. The research includes four parts. The second part is the research review of deformation and numerical analysis techniques for deep excavation engineering both domestically and internationally. The third part proposes a safety management design for SSDFP engineering using soil mechanics response simulation analysis. The first section analyzes the deformation characteristics of SSDFP based on soil mechanics response simulation. The second section designs a safety management plan for SSDFP engineering using soil mechanics response simulation analysis. The fourth part validated the safety management plan for SSDFP engineering using soil mechanics response simulation analysis.

2. Related works

Urban construction is currently a hot topic in the research field, and deep excavation engineering plays a crucial role in urban construction. Therefore, many researchers are committed to the study of deformation in deep excavation engineering and have achieved fruitful research results. Michalak H and other researchers proposed the use of spatial arrangement numerical simulation to construct a subsoil model in order to study the construction of a three-dimensional numerical model of adjacent buildings. The results showed that the three-dimensional computational model can draw actual affected map buildings and adjacent buildings in the designed new model, which is feasible [6]. Zhou L's research team proposed to conduct physical experiments using a deep buried drainage shield tunnel proposed in Shanghai to study the failure characteristics of segment lining under pressure. The results showed that the failure characteristics of shield lining were segment and ring joint waterproofing failure, and concrete cracking failure inside the lining [7].

Numerical analysis technology provides technical support for the design of deep excavation projects. In order to study the nonlinear stability characteristics of piezoelectric nanoplates, Rao R and other scholars proposed using numerical analysis techniques to track the nonlinear equilibrium curve of piezoelectric nanoplates within the framework of non local couple stress continuous elasticity. The results showed that this method is feasible [8]. Marode R.V. et al. proposed to use numerical analysis techniques to analyze the solid-state characteristics of workpieces in friction stir machining, and to refine the analysis of their microstructure. The results show that this method can analyze the transformation and temperature distribution of workpiece materials, and is effective [9].

In summary, although many experts have researched the deformation and numerical analysis techniques of deep excavation engineering, and have achieved rich results, only few utilized numerical analysis for the deformation characteristics of deep excavation engineering. Therefore, this study aims to investigate the safety management of deep excavation projects in subway stations by simulating the mechanical response of soil, in order to conduct deformation analysis of excavation in a more economical and accurate manner.

3. Design of safety management for deep excavation engineering of subway stations based on soil mechanics response simulation analysis

This chapter focuses on introducing the deformation characteristics of SSDFP based on soil mechanics response simulation, and combining with the example of SSDFP engineering in Wuhan, parameter optimization design is carried out, and a safety management plan for SSDFP engineering using soil mechanics response simulation analysis is proposed.

3.1. Deformation characteristics analysis of SSDFP using soil mechanics response simulation

Soil mechanics response simulation analysis refers to the use of numerical simulation technology to simulate the response and changes of soil under different mechanical conditions, to evaluate the physical, mechanical, and engineering properties of soil. Finite element method can be used to solve various complex geotechnical problems [10, 11]. The mathematical expression for the stability safety factor is shown in Equation (3.1).

$$F_s = \frac{S_u N_c}{D\left(W - \frac{S_u}{0.7K}\right)} \tag{3.1}$$

In Equation (3.1), F_s represents the stability safety factor. D represents the excavation depth, m. W represents the weight of the soil mass, kN/m3. K represents the width of the SSDFP. S_u represents the soil shear strength, kPa. N_c represents the stability coefficient. By considering the calculation of maximum GS and HD, the maximum surface settlement (SS) value around

the deep excavation project of the subway station can be obtained.According to the relevant principles of SS and HD of walls, combined with the elastic foundation method or the finite element method of the rod system, the SS can be calculated by the relationship between SS or HD and the area of ground movement. Therefore, in practical engineering, it is necessary to conduct detailed geological surveys and numerical simulation analysis based on specific geological conditions, construction methods, and enclosure structure forms to obtain accurate settlement calculation results. Figure 1 shows the deformation morphology of DFP settlement.

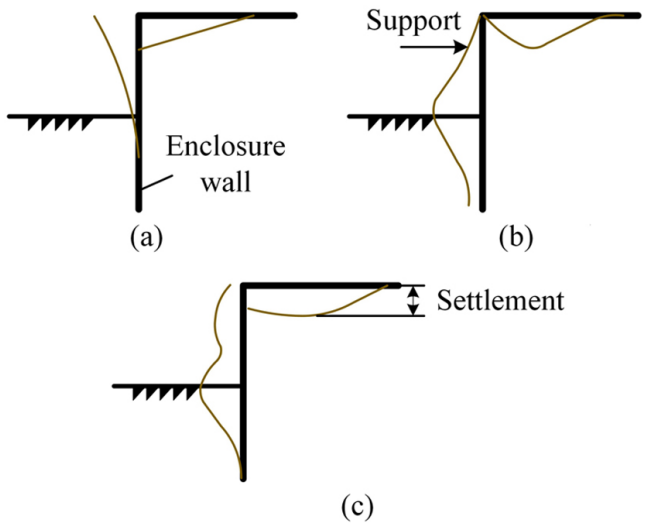

Fig. 1. Deformation morphology of DFP settlement: (a) Triangular settlement, (b) Parabolic settlement, (c) Trapezoidal settlement

From Figure 1, the settlement deformation of DFP can be manifested in three main forms: trapezoidal settlement, parabolic settlement, and triangular settlement. The mathematical expression for parabolic maximum settlement is shown in Equation (3.2).

$$S_{\max} = \frac{3.3KD^2W}{E_s y^3} x\,(y - x) \tag{3.2}$$

In Equation (3.2), $S_{\max}$ represents the parabolic maximum settlement. x and y represent the horizontal and vertical distance between the soil surface and the maximum settlement point, m. E_s represents the soil undrained modulus, MPa. The expression for the influence range of triangular settlement is shown in Equation (3.3).

$$e = H_g \tan(45^\circ - \phi/2) \tag{3.3}$$

In Equation (3.3), e represents the influence range of triangular settlement. H_g represents the retaining wall's height, and ϕ represents the average value of the friction angle between settlement and the soil surface. The mathematical expression for the maximum settlement of a

triangle is shown in Equation (3.4).

$$S'_{\max} = \frac{2S_{\max}}{e} \tag{3.4}$$

In Equation (3.4), $S'_{\max}$ represents the maximum settlement of a triangle, and the mathematical expression for the maximum settlement of a trapezoid is shown in Equation (3.5).

$$S''_{\max} = \frac{1.6S_{\max}}{e} - \frac{3\left(\Delta\delta_{w1} + \Delta\delta_{w2}\right)}{20} \tag{3.5}$$

In Equation (3.5), $S''_{\max}$ represents the maximum settlement of the trapezoid, $\Delta\delta_{w1}$ and $\Delta\delta_{w2}$ the HD of the top and bottom of the wall, respectively, m. The study combines the example of deep excavation engineering in Wuhan subway station and proposes a safety management process for deep excavation engineering in subway station using soil mechanics response simulation analysis, as shown in Figure 2.

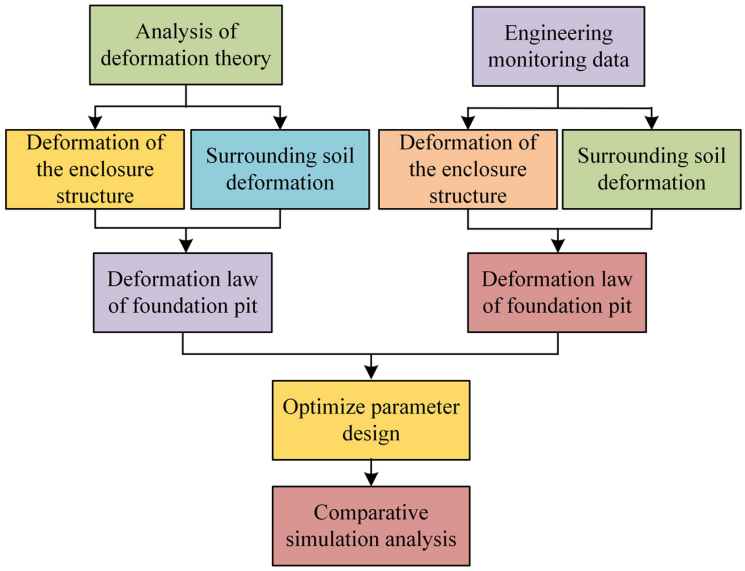

Fig. 2. Safety management process for deep excavation engineering of subway stations based on soil mechanics response simulation analysis

According to the safety management process of the SSDFP project shown in Figure 2, based on soil mechanics response simulation analysis, combined with deformation analysis theory and actual engineering monitoring data, in-depth analysis is conducted on the deformation of the retaining structure and surrounding soil obtained through research. Finally, the parameter design is optimized based on the deformation law, and the parameter optimization is simulated and compared for verification.

3.2. Design of safety management for deep excavation engineering of subway stations based on soil mechanics response simulation analysis

The Wuhan Metro Station DFP Project is located in Hankou District, Wuhan City. Its engineering geology mainly consists of artificial fill layers, Quaternary Holocene impact layers, and Paleogene Donghu Group bedrock. As a first-class safety level engineering project, its surrounding environment is complex, close to commercial areas, with numerous buildings and large traffic volume. In response to the above engineering characteristics, the project has chosen a combination of diaphragm wall support and supporting pile support for the combined enclosure structure. By utilizing steel and concrete supports, three steel pipe supports and three concrete supports are installed vertically in the DFP. The cross-section support diagram of the deep foundation pit is shown in Figure 3.

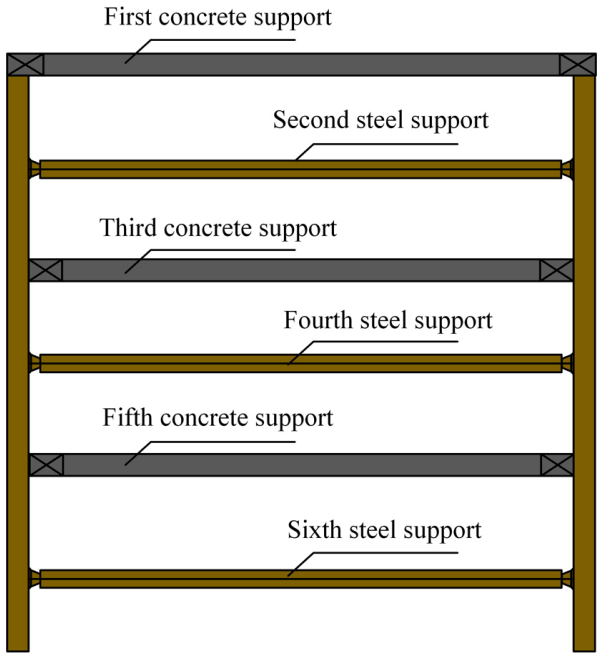

Fig. 3. Deep foundation pit section support diagram

A total of 1 steel pipe support and 6 concrete supports are installed vertically along the DFP in the shield tunnel section. The expression for the initial shear modulus of soil is shown in Equation (3.6).

$$F_0 = F_0^{\text{ref}} \left(\frac{\kappa \cos\phi + \sigma_3 \sin\phi}{\kappa \cos\phi + P^{\text{ref}} \sin\phi} \right)^{\psi} \tag{3.6}$$

In Equation (3.6), F_0 represents the initial shear modulus. P^{ref} represents the reference pressure. F_0^{ref} represents the initial shear modulus under the reference pressure. κ represents

the cohesion. ψ represents the power exponent, and σ_3 represents the principal stress [12, 13]. The relationship between shear modulus and initial shear model is shown in Equation (3.7).

$$\frac{F}{F_0} = \frac{1}{1 + |\gamma/\gamma_{0.7}|} \tag{3.7}$$

In Equation (3.7), F represents shear modulus. γ represents shear strain, and $\gamma_{0.7}$ represents ultimate shear strain. The shear strain is calculated in Equation (3.8).

$$\gamma = \frac{\sqrt{3}\,\|\varpi \Delta e\|}{\|\Delta e\|} \tag{3.8}$$

In Equation (3.8), ϖ represents the symmetric tensor of the strain history of the soil layer material, and Δe represents the increment of deviatoric strain. The corresponding shear strain is γ_c, as shown in Equation (3.9).

$$\gamma_c = \frac{1}{0.385}\left(\frac{F_0}{F_{\text{ur}}} - 1\right)\gamma_{0.7} \tag{3.9}$$

In Equation (3.9), F_{ur} represents the shear modulus when the soil displacement reaches the minimum value. The relationship between shear modulus and shear strain is shown in Equation (3.10).

$$F = \begin{cases} F_0\left(\dfrac{\gamma_{0.7}}{\gamma_{0.7} + 0.385\gamma}\right), & \gamma < \gamma_c \\ \dfrac{E_{\text{ur}}}{2\,(1 + \gamma_{0.7})}, & \gamma > \gamma_c \end{cases} \tag{3.10}$$

In Equation (3.10), E_{ur} represents the unloading and reloading modulus. The strain model of hardened soil is an improvement of the hardened soil model, and its basic theory is the same as that of the hardened soil model. Both are derived based on the relationship between biaxial stress and uniaxial strain under triaxial loading [14, 15]. The hyperbolic relationship between stress and strain is shown in Figure 4.

As shown in Figure 4, the stress-strain relationship exhibits a hyperbolic shape. This hyperbolic relationship is the foundation of the hardening soil model and the hardening soil strain model. Through this relationship, the stiffness of the soil can be calculated to determine whether the soil is in a small strain state. The hyperbolic relationship between stress and strain is shown in Equation (3.11).

$$\begin{cases} \varepsilon = \dfrac{1}{E_0} * \dfrac{q}{1 - q/q_0}, & q < q_f \\ E_0 = \dfrac{2E_{50}}{2 - P_f} \end{cases} \tag{3.11}$$

In Equation (3.11), ε represents the axial strain. E_0 represents the initial elastic modulus. q represents the deviator stress. q_f represents the ultimate deviator stress. q_0 represents the asymptotic value of shear strength. P_f represents the failure ratio, and E_{50} represents the

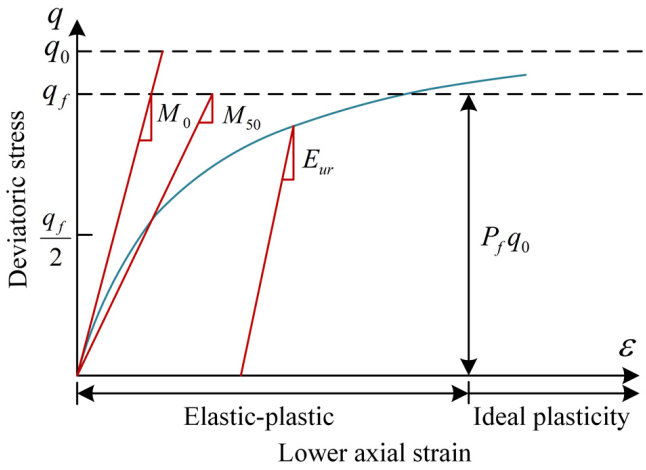

Fig. 4. The hyperbolic relationship between stress and strain

secant modulus of 50% of the ultimate load. The mathematical expression of E_{50} is shown in Equation (3.12).

$$E_{50} = E_{50}^{\text{ref}} \left(\frac{\kappa \cos\phi + \sigma_3 \sin\phi}{\kappa \cos\phi + P^{\text{ref}} \sin\phi} \right)^m \tag{3.12}$$

In Equation (3.12), E_{50}^{ref} represents the secant modulus under reference pressure P^{ref}, typically E_{50}^{ref} is defined as $100KPa$, and the actual modulus value depends on the principal stress σ_3 [16, 17]. The expression for the ultimate deviator stress is shown in Equation (3.13).

$$q_f = \frac{2\sin\phi\,(\kappa\cos\phi + \sigma_3)}{1 - \sin\phi} \tag{3.13}$$

In Equation (3.13), when q's value is equal to the ultimate deviator stress q_f, the failure criterion is met, and the soil undergoes complete plastic yield failure. The expression for the asymptotic value q_0 of shear strength at this point is shown in Equation (3.14).

$$q_0 = \frac{q_f}{P_f} \tag{3.14}$$

The unloading and reloading modulus E_{ur} reflects another type of stiffness modulus, as expressed in Equation (3.15).

$$E_{\text{ur}} = E_{\text{ur}}^{\text{ref}} \left(\frac{\kappa \cos\phi + \sigma_3 \sin\phi}{\kappa \cos\phi + P^{\text{ref}} \sin\phi} \right)^m \tag{3.15}$$

In Equation (3.15), $E_{\text{ur}}^{\text{ref}}$ represents the unloading and reloading modulus under reference pressure P^{ref}.

4. Optimization and verification of safety management parameters for SSDFP engineering based on soil mechanics response simulation analysis

This chapter established an experimental environment, providing a reliable experimental platform for subsequent optimization plans. Subsequently, a detailed analysis was conducted on the original vertical support plan for the DFP project of Wuhan Metro Station, and based on this, a preliminary parameter optimization plan was determined.

4.1. Analysis of the original design scheme for SSDFP engineering

To further improve the project safety and stability, optimization research on support parameters was conducted. On the basis of the original plan, the experiment attempted to increase and decrease a support, and numerical simulations were conducted on the settlement and displacement of the soil. In Figure 5(a), when 5 supports were increased to 6 supports, the settlement decreased from 30.0 mm to 24.2 mm, a decrease of 19.33%. When supports increased from 6 to 7, the settlement decreased from 24.2 mm to 19.9 mm, a decrease of 17.77%. In Figure 5(b), when 5 supports were increased to 6 supports, the HD decreased from 35.0 mm to 28.3 mm, a decrease of 19.14%. When supports increased from 6 to 7, the HD decreased from 28.3 mm to 24.9 mm, a decrease of 12.01%.

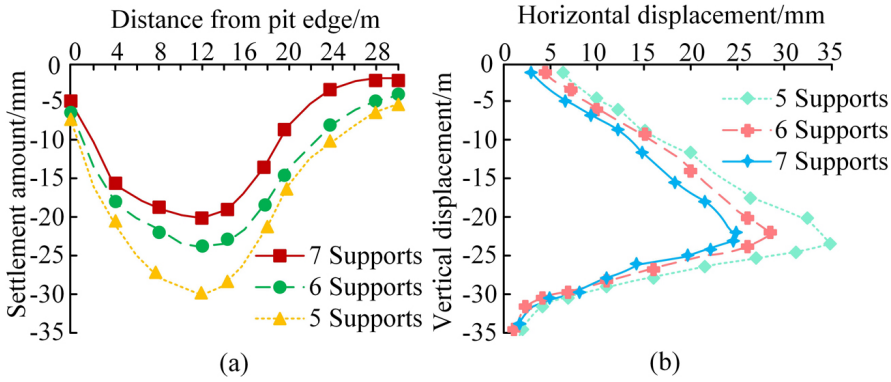

Fig. 5. Comparison of settlement (a) and displacement (b) results of soil

4.2. Verification of optimization plan for safety management parameters of SSDFP engineering

To improve the safety and efficiency of deep excavation engineering, this study considered the deformation of deep excavation and designed a parameter optimization plan. The comparison between the optimized parameter scheme and the actual engineering original scheme is shown in Table 1.

Table 1. Comparison between optimized parameter schemes and actual engineering original schemes

Parameter	Original plan	Optimization plan
Support form	The first, third, and fifth layers are supported by concrete, while the second, fourth, and sixth layers are supported by steel structures	The first, fourth, and fifth layers are supported by concrete, while the second, third, and sixth layers are supported by steel structures
Vertical spacing	6 m, 5 m, 5 m, 5 m, 5 m	6 m, 5 m, 4 m, 3.6 m, 3.5 m
Horizontal spacing	Concrete support 6 m, steel structure support 3 m	Concrete support 8 m, steel structure support 4 m

The comparison of settlement and displacement between the optimized parameter scheme and the original scheme is shown in Figure 6. In Figure 6(a), compared to the original scheme, the optimized parameter scheme reduced the settlement of the soil from 24.2 mm to 22.3 mm, a decrease of 7.85%. In Figure 6(b), compared to the original scheme, the optimized parameter scheme reduced the soil HD from 28.3 mm to 25.7 mm, a decrease of 9.18%.

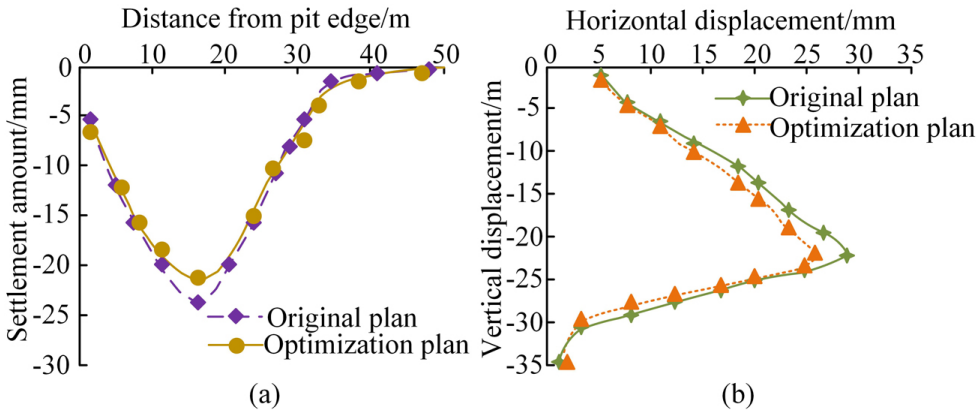

Fig. 6. Comparison of settlement (a) and displacement (b) of soil between the optimized parameter scheme and the original scheme

The comparison of horizontal displacement and moment stability between the two schemes is shown in Figure 7. In Figures 7(a) and 7(b), the maximum horizontal displacement of the original scheme reached 25.7 mm, while that of the optimized parameter scheme was only 18.6 mm, which was a decrease of 27.62% compared to the original scheme. In Figure 7(c) and Figure 7(d), the maximum positive and negative bending moment values of the original scheme were 1570.7 kN·m and 1054.5 kN·m, respectively, while those of the optimized parameter scheme were 1464.9 kN·m and 916.6 kN·m, respectively.

To further analyze the deformation safety of the project, numerical analysis was conducted on the middle deep excavation, and the shear force magnitude was compared as shown in

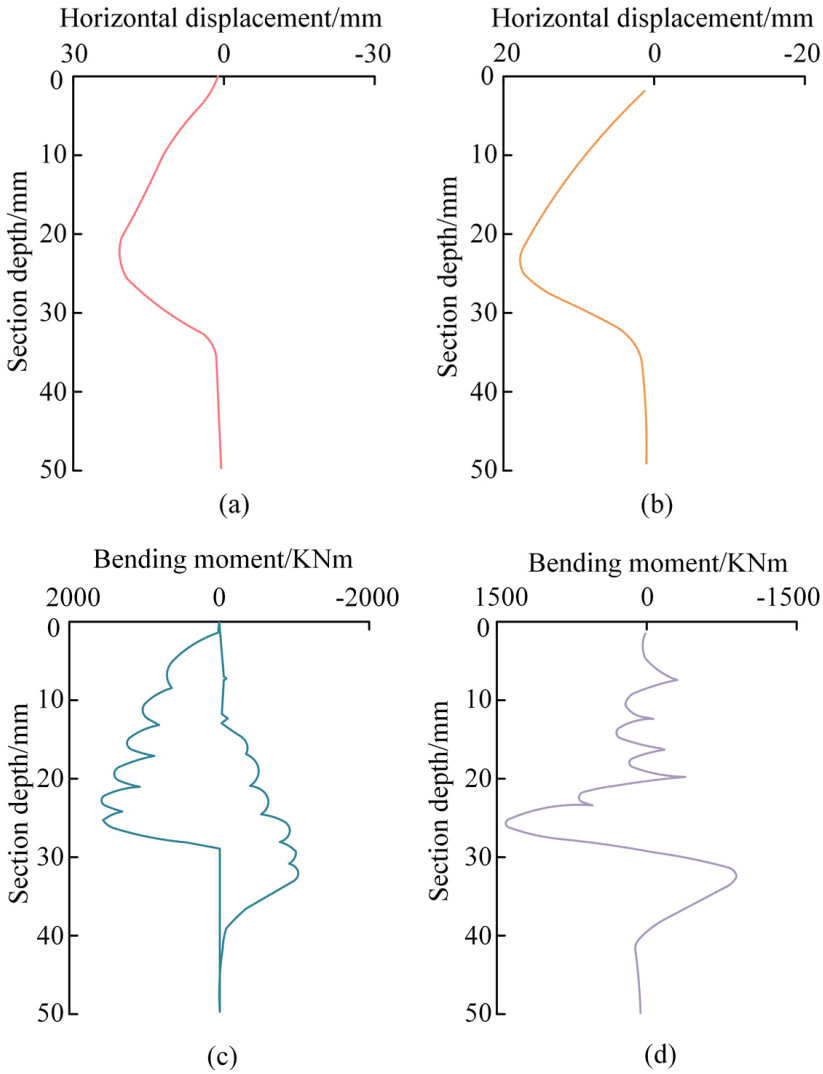

Fig. 7. Comparison of horizontal displacement and moment stability between two schemes: (a) Internal force displacement of the original plan, (b) Internal force displacement of optimization plan, (c) Comparison of bending moments of the original plan, (d) Comparison of bending moments of optimization plan

Figure 8. In Figure 8(a), the maximum shear positive value and maximum shear negative value of the original plan were 765.4 kN and 954.6 kN, respectively. In Figure 8(b), the maximum shear positive value and maximum shear negative value of the optimized parameter scheme were 615.9 kN and 749.8 kN, respectively. Compared with the original scheme, the maximum positive and negative shear force of the optimized parameter scheme were reduced by 149.5 kN and 204.8 kN, respectively.

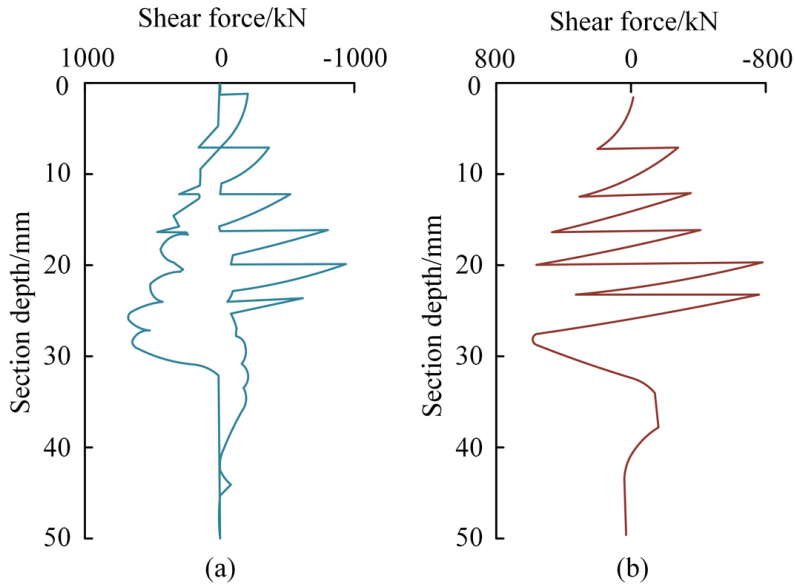

Fig. 8. Comparison of shear forces between two schemes: (a) Shear force analysis diagram of the original plan, (b) Shear force analysis diagram of the optimization plan

5. Conclusions

To balance the safety and economic benefits of subway station construction, this study uses the actual monitoring data of the DFP project of Wuhan subway station, combined with numerical analysis methods and deformation theory, to deeply analyze the deformation of surrounding soil and DFP support structure, and optimize the original plan based on this. Results indicated that the maximum horizontal displacement of the original scheme reached 25.7 mm, while that of the optimized parameter scheme was only 18.6 mm, which was a decrease of 27.62% compared to the original scheme. The maximum positive and negative bending moments of the optimized parameter scheme were 1464.9 kN·m and 916.6 kN·m, respectively, which were reduced by 105.8 kN·m and 137.9 kN·m compared to the original scheme's 1570.7 kN·m and 1054.5 kN·m, respectively. In summary, the safety management of SSDFP engineering using soil mechanics response simulation analysis has shown excellent performance in controlling DFP deformation, improving structural stress conditions, and reducing bending moment and shear peak values. However, the experiment only analyzed and discussed the factor of support position in deep excavation engineering, so the experimental results are not comprehensive enough, and this aspect still needs further improvement.

Acknowledgements

The research is supported by the Young Doctor Research Initiation Fund Project of Harbin University (No. HUDF2023102).

References

[1] Q. Zhang, "Deformation analysis of deep foundation pit excavation in China under time-space effect", *Geotechnical Research*, vol. 7, no. 3, pp. 146–152, 2020, doi: 10.1680/jgere.20.00009.

[2] M. Rasheed, A. Rashid, T. Rashid, S. H. A. Hamed, and O. A. A. AL-Farttoosi, "Application of numerical analysis for solving nonlinear equation", *Journal of Al-Qadisiyah for Computer Science and Mathematics*, vol. 13, no. 3, pp. 70–78, 2021, doi: 10.29304/jqcm.2021.13.3.844.

[3] G. Prieto, Á. G. Andrade, and D. M. Martínez, "Numerical analysis of histogram-based estimation techniques for entropy-based spectrum sensing", *IETE Technical Review*, vol. 37, no. 1, pp. 91–97, 2020, doi: 10.1080/02564602.2019.1566029.

[4] S. Kaewunruen, S. Peng, and O. Phil-Ebosie, "Digital twin aided sustainability and vulnerability audit for subway stations", *Sustainability*, vol. 12, no. 19, art. no. 7873, 2020, doi: 10.3390/su12197873.

[5] Z. Zhong, Y. Shen, M. Zhao, L. Li, and X. Du, "Seismic performance evaluation of two-story and three-span subway station in different engineering sites", *Journal of Earthquake Engineering*, vol. 26, no. 14, pp. 7505–7535, 2022, doi: 10.1080/13632469.2021.1964647.

[6] P. Popielski, B. Bednarz, T. Majewski, and M. Niedostatkiewicz, "Settlement of a historic building due to seepage-induced soil deformation", *Archives of Civil Engineering*, vol. 69, no. 2, pp. 65–82, 2023, doi: 10.24425/ace.2023.145253.

[7] L. Zhou, H. Zhu, Y. Shen, L. Guan, Z. Yan, W. Sun, and Y. Li, "Full-scale experimental investigation on progressive failure characteristics of shield segmental lining connected through segmental joints containing ductile-iron joint panels", *Archives of Civil and Mechanical Engineering*, vol. 22, no. 3, art. no. 120, 2022, doi: 10.1007/s43452-022-00438-0.

[8] R. Rao, Z. Ye, Z. Yang, S. Sahmani, and B. Safaei, "Nonlinear buckling mode transition analysis of axial-thermal-electrical-loaded FG piezoelectric nanopanels incorporating nonlocal and couple stress tensors", *Archives of Civil and Mechanical Engineering*, vol. 22, no. 3, art. no. 125, 2022, doi: 10.1007/s43452-022-00437-1.

[9] R. V. Marode, S. R. Pedapati, T. A. Lemma, and M. Awang, "A review on numerical modelling techniques in friction stir processing: current and future perspective", *Archives of Civil and Mechanical Engineering*, vol. 23, no. 3, art. no. 154, 2023, doi: 10.1007/s43452-023-00688-6.

[10] X. Yang, R. Zhang, Y. Li, and F. Pan, "Passenger evacuation path planning in subway station under multiple fires based on multiobjective robust optimization", *IEEE Transactions on Intelligent Transportation Systems*, vol. 23, no. 11, pp. 21915–21931, 2022, doi: 10.1109/TITS.2022.3190291.

[11] H. Zhuang, J. Ren, Y. Miao, L. Jing, E. Yao, and C. Xu, "Seismic performance levels of a large underground subway station in different soil foundations", *Journal of Earthquake Engineering*, vol. 25, no. 14, pp. 2808–2833, 2021, doi: 10.1080/13632469.2019.1651423.

[12] S. Ahmad, A. Ullah, A. Akgül, and D. Baleanu, "Theoretical and numerical analysis of fractal fractional model of tumor-immune interaction with two different kernels", *Alexandria Engineering Journal*, vol. 61, no. 7, pp. 5735–5752, 2022, doi: 10.1016/j.aej.2021.10.065.

[13] A. I. K. Butt, W. Ahmad, M. Rafiq, and D. Baleanu, "Numerical analysis of Atangana-Baleanu fractional model to understand the propagation of a novel corona virus pandemic", *Alexandria Engineering Journal*, vol. 61, no. 9, pp. 7007–7027, 2022, doi: 10.1016/j.aej.2021.12.042.

[14] Y. Fang, B. Luo, T. Zhao, D .He, B. Jiang, and Q. Liu, "ST-SIGMA: Spatio-temporal semantics and interaction graph aggregation for multi-agent perception and trajectory forecasting", *CAAI Transactions on Intelligence Technology*, vol. 7, no. 4, pp. 744–757, 2022, doi: 10.1049/cit2.12145.

[15] C. Hebbi and H. R. Mamatha, "Comprehensive dataset building and recognition of isolated handwritten kannada characters using machine learning models", *Artificial Intelligence and Applications*, vol. 1, no. 3, pp. 179–190, 2023, doi: 10.47852/bonviewAIA3202624.

[16] S. Pal, A. Roy, P. Shivakumara, and U. Pal, "Adapting a swin transformer for license plate number and text detection in drone images", *Artificial Intelligence and Applications*, vol. 1, no. 3, pp. 145–154, 2023, doi: 10.47852/bonviewAIA3202549.

[17] C. Oh, "Exploring the way to harmonize sustainable development assessment methods in article 6.2 cooperative approaches of the Paris agreement", *Green and Low-Carbon Economy*, vol. 1, no. 3, pp. 121–129, 2023, doi: 10.47852/bonviewGLCE32021065.

Received: 2023-12-04, Revised: 2024-03-26